Journal of Magnetism and Magnetic Materials 323 (2011) 569–573

Contents lists available at ScienceDirect

Journal of Magnetism and Magnetic Materials

journal homepage: www.elsevier.com/locate/jmmm

Fuel additives and heat treatment effects on nanocrystalline zinc ferrite phase composition

Ping Hu [a], De-an Pan [a], Xin-feng Wang [b], Jian-jun Tian [a], Jian Wang [a], Shen-gen Zhang [a,*], Alex A. Volinsky [c]

[a] School of Materials Science and Engineering, University of Science and Technology Beijing, Beijing 100083, P.R. China
[b] Beijing Electronic Science Vocational College, Beijing 100026, P.R. China
[c] Department of Mechanical Engineering, University of South Florida, Tampa, FL 33620, USA

ARTICLE INFO

Article history:
Received 15 January 2010
Received in revised form
11 October 2010
Available online 28 October 2010

Keywords:
Zinc ferrite
Fuel additive
Heat treatment
Phase composition

ABSTRACT

Nanocrystalline $ZnFe_2O_4$ powder was prepared by the auto-combustion method using citric acid, acetic acid, carbamide and acrylic acid as fuel additives. Pure spinel zinc ferrite with the crystallite size of about 15 nm can be obtained by using acrylic acid as fuel additive. Samples prepared using other fuel additives contain ZnO impurities. In order to eliminate ZnO impurities, the sample prepared with citric acid as fuel additive was annealed at different temperatures up to 1000 °C in air and in argon. Annealed powders have pure $ZnFe_2O_4$ phase when annealing temperature is higher than 650 °C in air. Sample annealed at 650 °C in air is paramagnetic. However, annealed powders become a mixture of Fe_3O_4 and FeO after annealing at 1000 °C in argon atmosphere due to Zn volatility and the reduction reaction.

1. Introduction

Zinc ferrite ($ZnFe_2O_4$) has normal spinel structure; it is a commercially important material and has been widely used in magnetic applications [1,2], gas sensors [3], catalysts [4], photocatalysts [5,6] and absorbent materials [7,8] because of its excellent electrical and magnetic properties.

Recently, nanocrystalline ferrites have been extensively studied because of their superior physical and chemical properties compared with bulk counterparts [9,10]. To prepare high electromagnetic performance zinc ferrites, various synthesizing methods have been reported, including high-energy ball milling [1–2], hydrothermal technique [4], co-precipitation [11,12], ferrocenyl precursor method [13], ultrasonic cavitation [14], thermal plasma [15], etc. However, some of these methods encountered problems such as the requirement of complicated equipment or long processing time caused by multiple steps, thus being economically unfeasible for large-scale production. Lately more attention has been paid to the auto-combustion method, which is an exothermic redox reaction between metal nitrates (oxidizing agents) and appropriate fuel additives (reducing agents) and had been successfully used for synthesizing nanocrystalline ferrites [16]. The advantages of this method are chemically homogeneous composition, processing simplicity, low energy loss, high-production efficiency and high-purity products [17].

The auto-combustion method has been demonstrated for zinc ferrite production [18–22]. However, few studies considered the influence of fuel additives and heat treatment conditions on the phase composition of nanocrystalline zinc ferrite. In the present work, nanocrystalline zinc ferrite was prepared by the auto-combustion method using citric acid, acetic acid, carbamide, and acrylic acid as fuel additives. The effects of different fuel additives on crystallite phase composition and microstructure of zinc ferrite were characterized. Then as-prepared powders were annealed at different temperatures ranging up to 1000 °C for 1 h in air and in argon. Influence of heat treatment conditions on microstructure and magnetic properties of annealed zinc ferrites were investigated.

2. Experiment

Nanocrystalline zinc ferrite ($ZnFe_2O_4$) was prepared by the auto-combustion method using ferric nitrate $Fe(NO_3)_3 \cdot 9H_2O$, zinc nitrate $Zn(NO_3)_2 \cdot 6H_2O$ as raw materials and citric acid $C_6H_8O_7 \cdot H_2O$, acetic acid CH_3COOH, carbamide $CO(NH_2)_2$, and acrylic acid C_2H_3COOH as fuel additives for samples labeled S1, S2, S3 and S4, respectively. Appropriate proportion of metal nitrates and fuel additives were dissolved in distilled water, and the solution pH value was adjusted to 7 with ammonia. The solution was heated to 60 °C and continuously stirred using magnetic agitation. After 4 h the solution became a homogeneous viscous gel. Then the gel was oven dried at 120 °C for 24 h to obtain a dried gel. A loose and very fine zinc ferrite powder was produced after the dried gel had spontaneously combusted in air.

* Corresponding author. Tel./fax: +86 10 62333375.
E-mail address: zhangshengen@mater.ustb.edu.cn (S.-g. Zhang).

0304-8853/$ - see front matter © 2010 Elsevier B.V. All rights reserved.
doi:10.1016/j.jmmm.2010.10.013

In order to investigate the influence of annealing temperature on structural and magnetic properties, as-prepared auto-combusted S1 powders were annealed between 300 and 1000 °C for 1 h in air and in argon.

X-ray diffraction (XRD) was used to determine the phases and crystallite size. XRD patterns were recorded on a Philips APD-10 diffractometer using Cu radiation. The morphology of particles was observed by scanning electron microscopy (SEM) (LEO 1450). LDJ 9600 (LDJ Electronics, Troy, MI, USA) vibrating sample magnetometer (VSM) was used to investigate the magnetic properties at room temperature.

3. Results and discussion

3.1. Phase analysis of products with different fuel additives

The dried gel for sample S4 combusted rapidly and more intense than S1 during its ignition in air. However, the dried gel for sample S2 and S3 began to smoke after 2–3 min preheating and combusted slowly and mildly. Fig. 1 shows the XRD patterns for samples S1, S2, S3 and S4 with different fuel additives. These measurements show that only S4 has a pure spinel zinc ferrite structure (JCPDS # 22-1012) by gel precursor auto-combustion, and samples S1, S2 and S3 contain XRD reflections coming from impurities due to the ZnO phase (JCPDS # 36-1451).

The synthesis of $ZnFe_2O_4$ by auto-combustion can be explained as follows. Dried gels first generate metal oxide ZnO and Fe_3O_4 in the beginning of the combustion process. Combustion releases large amounts of heat, and the following combination reaction occurs:

$$6ZnO + 4Fe_3O_4 + O \rightarrow 6ZnFe_2O_4 \quad (1)$$

The sample S4 has pure $ZnFe_2O_4$ phase due to intense combustion and large amount of heat, so reaction (1) for sample S4 fully completes and produces pure $ZnFe_2O_4$. However, samples S1, S2 and S3 retain some ZnO phase due to their mild combustion and incomplete reaction (1). Moreover, Fe_3O_4 can form a solid solution with $ZnFe_2O_4$ for the same spinel structure, but ZnO cannot be dissolved in $ZnFe_2O_4$ due to its hexagonal crystal structure. Therefore, ZnO remains in samples S1, S2 and S3 as a separate hexagonal phase.

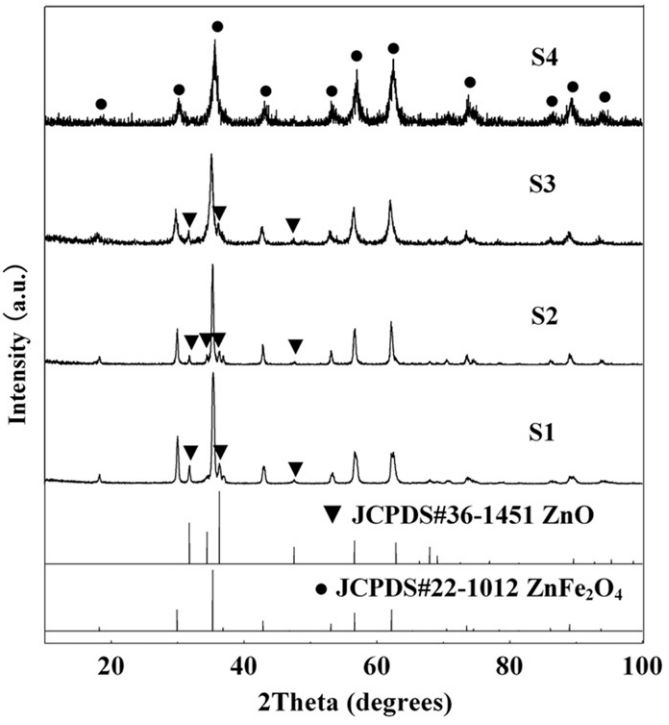

Fig. 1. XRD patterns for samples S1, S2, S3 and S4.

Table 1 shows the crystallite sizes and phases of all samples in our experiments. The crystallite sizes were determined using Debye–Scherrer's formula [23]. The crystallite size of pure $ZnFe_2O_4$ sample S4 is about 15 nm. Owing to the intense and rapid combustion using acrylic acid as fuel additive, the crystallite does not have enough time to grow, so the crystallite size of S4 is quite small. However, acrylic acid also causes imperfect crystallization and lower crystallinity for sample S4 (Fig. 1). Therefore, it is very important to select the appropriate fuel additives for phase formation by the auto-combustion method.

3.2. Heat treatment in air

In order to eliminate ZnO impurities and obtain pure $ZnFe_2O_4$ from samples S1, S2, S3, we chose S1 as a representative sample and subsequently annealed it at different temperatures ranging from 400 to 1000 °C for 1 h in air. The XRD patterns of annealed products are shown in Fig. 2. Below 650 °C annealing temperature, powder has ZnO phase. However, powders have pure spinel $ZnFe_2O_4$ structure when the annealing temperature is higher than 650 °C. Moreover, with higher annealing temperature, powders have stable structure and fine crystallization. The crystallite sizes of annealed powder increase from 27.7 to 52.5 nm with the annealing temperature increase from 400 to 1000 °C (Table 1).

Nanocrystalline ferrites produced by the auto-combustion method have large specific surface area and good reactivity [17]. Annealed powders are pure $ZnFe_2O_4$ and ZnO disappeared when the annealing temperature was higher than 650 °C due to the combination reaction (1) at 650 °C. However, annealed powders also have ZnO impurity phase below 650 °C (400 and 600 °C annealing temperatures), possibly due to very slow diffusion rate at lower temperatures.

3.3. Heat treatment in argon

The structure of ferrite depends on the environment and the heat treatment temperature [16]. Sample S1 was annealed at different temperatures ranging from 300 to 1000 °C for 1 h in argon atmosphere and the resulting XRD patterns are shown in Fig. 3. The products contain a mixture of $ZnFe_2O_4$ and ZnO phases when sample S1 was annealed below 1000 °C in argon. However, annealed powders become a mixture of Fe_3O_4 (JCPDS # 19-0629)

Table 1
Crystallite size and phases for all samples.

Samples	Crystallite size (nm)	Phase
S1	23.4	$ZnFe_2O_4$ and ZnO
S2	29.2	$ZnFe_2O_4$ and ZnO
S3	20.3	$ZnFe_2O_4$ and ZnO
S4	15.1	$ZnFe_2O_4$
S1 annealed at 400 °C in air	27.7	$ZnFe_2O_4$ and ZnO
S1 annealed at 600 °C in air	35.1	$ZnFe_2O_4$ and ZnO
S1 annealed at 650 °C in air	35.9	$ZnFe_2O_4$
S1 annealed at 700 °C in air	39.6	$ZnFe_2O_4$
S1 annealed at 800 °C in air	44.1	$ZnFe_2O_4$
S1 annealed at 1000 °C in air	52.5	$ZnFe_2O_4$
S1 annealed at 300 °C in Ar	25.6	$ZnFe_2O_4$ and ZnO
S1 annealed at 500 °C in Ar	35.9	$ZnFe_2O_4$ and ZnO
S1 annealed at 650 °C in Ar	39.2	$ZnFe_2O_4$ and ZnO
S1 annealed at 800 °C in Ar	55.8	$ZnFe_2O_4$ and ZnO
S1 annealed at 1000 °C in Ar	39.7	Fe_3O_4 and FeO

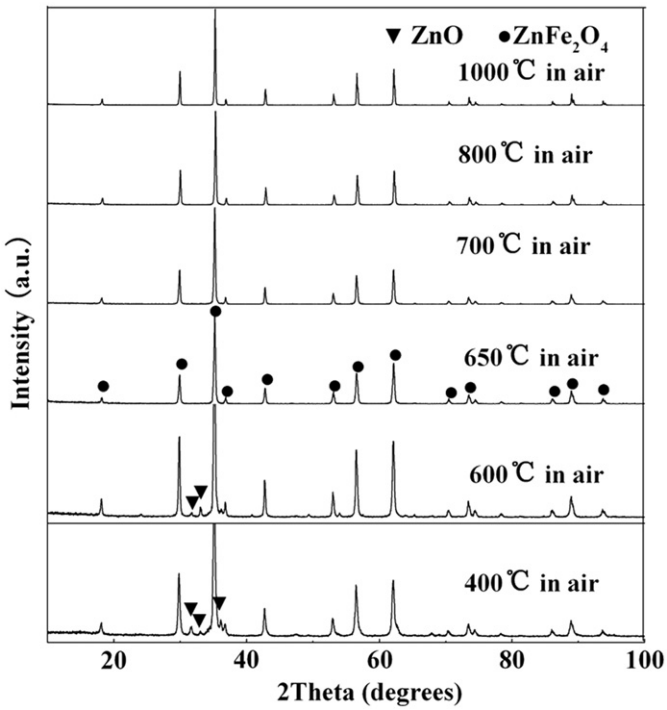

Fig. 2. XRD patterns for sample S1 annealed at different temperatures in air.

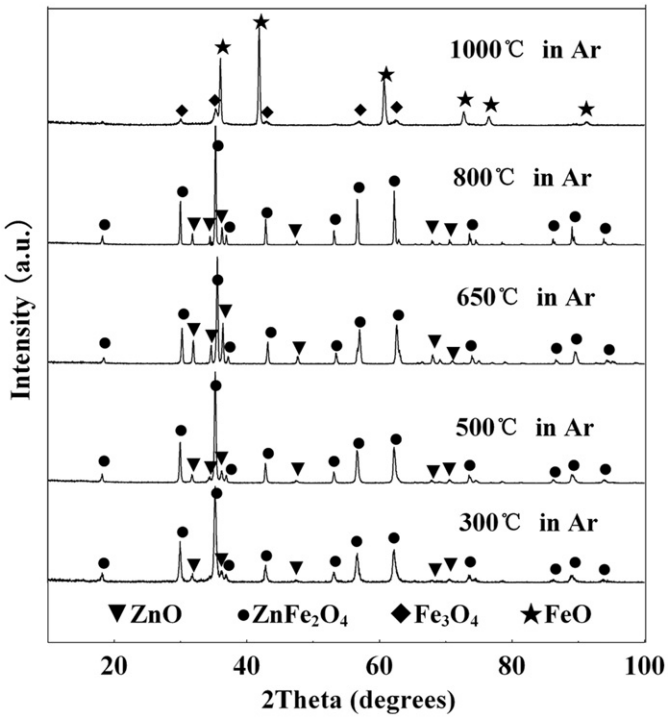

Fig. 3. XRD patterns for sample S1 annealed at different temperatures in argon.

and FeO (JCPDS # 06-0615) after annealing at 1000 °C in argon atmosphere due to Zn volatility in the samples.

Normally it is impossible to remove ZnO from ferrite because of the 1975 °C melting point of bulk ZnO. The following decomposition reaction in ZnO would occur with increased annealing temperature [24]

$$ZnO \rightarrow Zn + 1/2O_2 \quad (2)$$

It causes Zn to dissociate from ZnO, and the boiling point of Zn is 907 °C. Thus, Zn would be volatile if it dissociated from ZnO during preparation and heat treatment of zinc ferrites. It is hard to get rid of Zn in ferrites due to Zn^{2+} fixed in zinc ferrite lattice for $ZnFe_2O_4$ compound which is combined with ZnO and Fe_3O_4. However, $ZnFe_2O_4$ conversion takes place at high annealing temperature [25]:

$$ZnFe_2O_4 \rightarrow (1-x)ZnFe_2O_4 + 2/3xFe_3O_4 + xZnO + 1/6xO_2 \quad (3)$$

In other words, ZnO can partially dissociate from $ZnFe_2O_4$ at high annealing temperature due to reaction (3) and its hexagonal structure. This free ZnO then decomposes by reaction (2), which removes Zn from the samples. The higher the annealing temperature, the more Zn is removed. Moreover, both reactions (2) and (3) are oxygen evolution reactions; therefore they will aggravate Zn volatility in anoxic atmosphere.

In our experiments Zn is volatilized because samples annealed in argon atmosphere accelerate reactions (2) and (3). As a result Zn volatilization increases with annealing temperature in argon atmosphere. At 1000 °C annealing temperature, powders have Fe_3O_4 and FeO phases due to complete Zn volatilization and further reduction in argon atmosphere.

Fig. 4 shows the effect of the annealing temperature on the crystallite size of annealed S1 sample in argon. It shows that the crystallite sizes of annealed powders increased from 25.6 to 55.8 nm with the annealing temperature increase from 300 to 800 °C. However, it decreased to 39.7 nm at 1000 °C due to decomposition and reduction in ferrites.

3.4. Products microstructure evolution with different fuel additives

Typical SEM micrographs of samples S1, S2, S3 and S4 microstructure are shown in Fig. 5. It is clear that sample S4 is uniform in both morphology and particle size due to the intense and rapid combustion using acrylic acid as fuel additive. However, samples S1, S2 and S3 are non-uniform in morphology and are agglomerated to some extent due to their slow and mild combustion and ZnO impurities.

3.5. Magnetic properties

Magnetic properties were measured by the VSM at room temperature for the sample S1 annealed at 650 °C in air, as shown in Fig. 6.

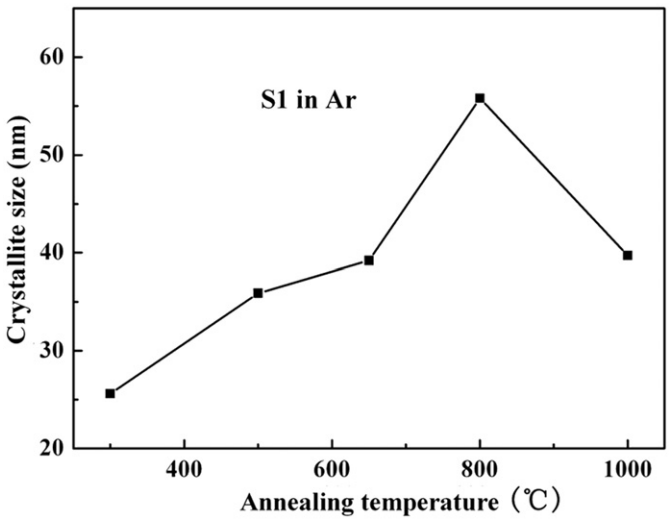

Fig. 4. S1 crystallite size dependence on the annealing temperature in argon atmosphere.

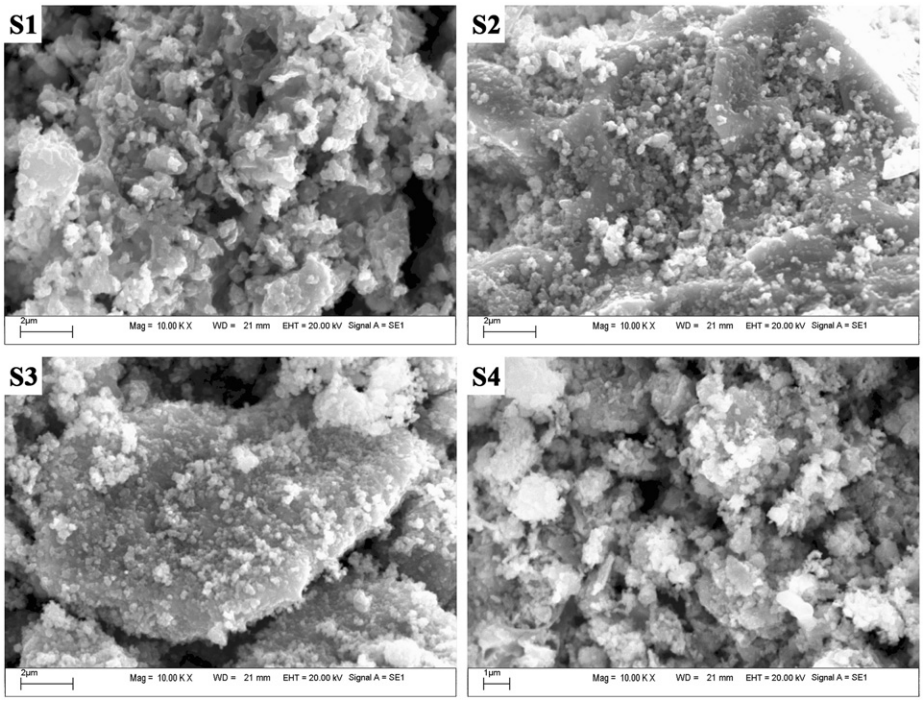

Fig. 5. SEM micrographs for samples S1, S2, S3 and S4.

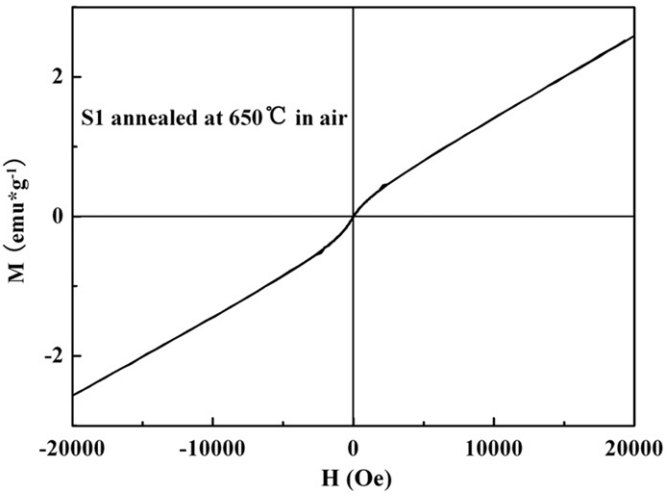

Fig. 6. Magnetic hysteresis loops for sample S1 annealed at 650 °C in air.

Table 2
Magnetic properties, crystallite size and phases of S1 annealed at 650 °C in air.

Samples	M_s (emu g^{-1})	M_r (emu g^{-1})	H_c (Oe)	Crystallite size (nm)	Phase
A annealed at 650 °C in air	2.583	5.551×10^{-3}	15	35.9	Zinc ferrite

Magnetic properties, crystallite size and phases of sample S1 annealed at 650 °C in air are listed in Table 2. It is clear that $ZnFe_2O_4$ has good paramagnetism. The magnetization value does not attain saturation at the highest employed magnetic field of 20 kOe. A magnetization value of 2.583 emu g^{-1} was obtained at room temperature. No magnetic anisotropy was observed. The paramagnetic properties for $ZnFe_2O_4$ in our experiment ($M_r = 5.551 \times 10^{-3}$ emu g^{-1}) are superior to the nanocrystalline zinc ferrite samples prepared by other techniques [12,26–30]. Taking into account normal spinel structure of zinc ferrite ($ZnFe_2O_4$) which has a tetrahedral A-site occupied by Zn^{2+} ions and an octahedral B-site occupied by Fe^{3+} ions; the coercivity value of 15 Oe suggests that in the as-prepared zinc ferrite cation distribution has partially changed from normal to mixed spinel type. This can be attributed to some Fe^{3+} ions occupying tetrahedral A-sites and switch by the A–B super-exchange interaction [26,31].

4. Conclusions

Nanocrystalline $ZnFe_2O_4$ was prepared by the auto-combustion method using different fuel additives. Pure spinel zinc ferrite can be obtained by using only acrylic acid as fuel additive, with the crystallite size of about 15 nm and uniform in both morphology and particle size due to intense and rapid combustion. However, the samples obtained using other fuel additives contain ZnO impurities.

In order to eliminate ZnO impurities, sample S1 was annealed at different temperatures ranging from 400 to 1000 °C for 1 h in air and in argon. Annealed powders have pure $ZnFe_2O_4$ when the annealing temperature is higher than 650 °C in air. With continuously increased annealing temperature, powders have stable structure and fine crystallization in air. Sample S1 annealed at 650 °C in air has good paramagnetism. However, annealed powders become a mixture of Fe_3O_4 and FeO after annealing at 1000 °C in argon atmosphere due to the volatilization of Zn and the reduction reaction in argon atmosphere.

Acknowledgments

The authors gratefully acknowledge support provided by the National Natural Science Foundation of China (no. 50972013, no. 50874010 & no. 50802008), National Key Project of Scientific and Technical Supporting Programs funded by Ministry of Science & Technology of China (no. 2009BAE74B03) and Guangdong Province

& Ministry of Education Industry-Study-Research United project of China (no. 2007B090400108, no. 2008B090500036).

References

[1] H. Ehrhardt, S.J. Campbel, M. Hofmann, Scr. Mater. 48 (2003) 1141.
[2] S. Bid, S.K. Pradhan, Mater. Chem. Phys. 82 (2003) 27.
[3] N. Ikenag, Y. Ohgaito, H. Matsushima, T. Suzuki, Fuel 83 (2004) 661–669.
[4] J.A. Toledo-Antonio, N. Nava, M. Martínez, X. Bokhimi, Appl. Catal. A Gen. 234 (2002) 137.
[5] F. Papa, L.a Patron, O. Carp, C. Paraschiv, B. Ioan, J. Mol. Catal. A: Chem. 299 (2009) 93–97.
[6] G.L. Fan, Z.J. Gu, L. Yang, F. Li, Chem. Eng. J. 155 (2009) 534–541.
[7] M. Kobayashi, H. Shirai, M. Nunokawa, Energy Fuels 16 (2002) 1378.
[8] F. Tomás-Alonso, J.M.Palacios Latasa, Fuel Process. Technol. 86 (2004) 191.
[9] S.D. Shenoya, P.A. Joyb, M.R. Anantharaman, J. Magn. Magn. Mater. 269 (2004) 217–226.
[10] E.J. Choi, Y. Ahn, K.C. Song, J. Magn. Magn. Mater. 301 (2006) 171–174.
[11] R. Klimkiewicz, J. Wolska, A. Przepiera, K. Przepiera, M. Jabłoński, S. Lenart, Mater. Res. Bull. 44 (2009) 15–20.
[12] A. Kundu, C. Upadhyay, H.C. Verma, Phys. Lett. A 311 (2003) 410–415.
[13] J.A. Zhao, L.W. Mi, H.W. Hou, X.J. Shi, Y.T. Fan, Mater. Lett. 61 (2007) 4196–4198.
[14] M. Sivakumar, A. Towata, K. Yasui, T. Tuziuti, Y. Iida, Curr. Appl. Phys. 6 (2006) 591–593.
[15] I. Mohai, J. Szépvölgyi, I. Bertóti, M. Mohai, J. Gubicza, T. Ungár, Solid State Ionics 141-142 (2001) 163–168.
[16] P. Hu, H.B. Yang, D.A. Pan, H. Wang, J.J. Tian, S.G. Zhang, X.F. Wang, A.A. Volinsky, J. Magn. Magn. Mater. 322 (2010) 173–177.
[17] A. Verma, R. Chatterjee, J. Magn. Magn. Mater. 306 (2006) 313–320.
[18] A. Kundu, S. Anand, H.C. Verma, Powder Technol. 132 (2003) 131–136.
[19] J.P. Singh, R.C. Srivastava, H.M. Agrawal, R.P.S. Kushwaha, P. Chand, R. Kumar, Int. J. Nanosci. 7 (2008) 21–27.
[20] M.R. Anantharaman, S. Jagatheesan, K.A. Malini, S. Sindhu, A. Narayanasamy, C.N. Chinnasamy, J.P. Jacobs, S. Reijne, K. Seshan, R.H.H. Smits, H.H. Brongersma, J. Magn. Magn. Mater. 189 (1998) 83–88.
[21] J. Xiang, X. Shen, Y. Zhu, X. Meng, J. Jiangsu Univ. (Natural Science Edition) 30 (2009) 36–39.
[22] R. Zhang, J. Huang, J. Zhao, Z. Sun, Y. Wang, Energy Fuels 21 (2007) 2682–2687.
[23] H.P. Klug, L.E. Alexander, X-ray Diffraction Procedures for Polycrystalline and Amorphous Materials, John Wiley and Sons, New York, 1997, p. 637.
[24] Z.G. Zhou, Ferrite Magnetic Materials, Science Press, Beijing, 1981, p. 376.
[25] Y. Takahashi, H. Aoki, H. Kaneko, N. Hasegawa, A. Suzuki, Y. Tamaura, Solid State Ionics 172 (2004) 89–91.
[26] F.A. López, A. López-Delgado, J.L. Martín de Vidales, E. Vila, J. Alloys Compd. 265 (1998) 291–296.
[27] J.P. Muñoz Mendoza, O.E. Ayala Valenzuela, V. Corral Flores, J. Matutes Aquino, S.D. De la Torre, J. Alloys Compd. 369 (2004) 144–147.
[28] S.X. Liu, B. Yue, K. Jiao, Y. Zhou, H.Y. He, Mater. Lett. 60 (2006) 154–158.
[29] N. Wakiya, K. Muraoka, T. Kadowaki, T. Kiguchi, N. Mizutani, H. Suzuki, K. Shinozaki, J. Magn. Magn. Mater. 310 (2007) 2546–2548.
[30] A.G. Yan, X.H. Liu, R.R. Shi, N. Zhang, R. Yi, Y.B. Li, G.H. Gao, G.Z. Qiu, Solid State Commun. 146 (2008) 483–486.
[31] H. Xue, Z.H. Li, X.X. Wang, X.Z. Fu, Mater. Lett. 61 (2007) 347–350.